NASA TECHNICAL MEMORANDUM 102751

MATRIX FATIGUE CRACK DEVELOPMENT IN A NOTCHED CONTINUOUS FIBER SCS-6/Ti-15-3 COMPOSITE

B. M. Hillberry and W. Steven Johnson

NOVEMBER 1990

Prepared for the
Symposium on Microcracking Induced
Damage in Composites
1990 ASME Winter Annual Meeting
Dallas, Texas, November 26-28, 1990

National Aeronautics and
Space Administration

Langley Research Center
Hampton, Virginia 23665-5225

ERRATA

NASA Technical Memorandum 102751

MATRIX FATIGUE CRACK DEVELOPMENT IN A NOTCHED CONTINUOUS FIBER SCS-6/Ti-15-3 COMPOSITE

B. M. Hillberry and W. Steven Johnson

November 1990

Equations (9) and (10) on page 5 were incorrect. Replace pages 5 and 6 with the attached corrected pages.

Issued December 1990

INTRODUCTION

Continuous silicon fibers in a titanium matrix provide a high stiffness, high strength composite system. In contrast to polymer matrix composites, the metal matrix carries a significant portion of the load. As fatigue cracks develop in the matrix there can be a significant reduction in composite stiffness as well as strength. Because of the load transfer between the fiber and the matrix in this system, the fiber-matrix interface becomes more critical.

In room temperature tests of unnotched SCS-6/Ti-15-3 composite specimens with a variety of layups, Johnson et al. (1990), observed fatigue failure of the fibers but not the matrix except for one long life test. They also showed that the fatigue life correlated well with the stress range in the zero-degree fiber. This indicates that at higher stress levels the fatigue life of the fibers is less than that of the matrix.

Unlike the smooth configuration, notched specimens (double edge notch and center hole) tested by Naik and Johnson (1991) showed multiple matrix fatigue cracks emanating from the notch and an overall uniform fatigue crack spacing (Figure 1). In addition, fiber-matrix interface separation extending from the matrix fatigue crack and progressing along the fiber was observed near the notch (Figure 2). Harmon et al. (1987) observed similar uniform matrix fatigue crack spacing in center hole notched specimens.

In the $[90]_8$ laminate of this same composite a significant decrease in stiffness (knee) has been observed in the stress-strain curve at a stress level well below matrix yield. This was found to be associated with fiber-matrix interface failure due to the tensile stress acting normal to the interface. Fiber-matrix interface separation was verified using the replica technique on the specimen edge. The knee has been observed to exist upon unloading, indicating that the crack is closing around the fiber due to matrix residual stresses. The calculated thermal residual stresses due to processing correlate well with the magnitude of the knee (Johnson et al., 1990). It is thought that fatigue cracks may initiate at the 90 degree fiber due to this fiber-matrix separation and then propagate through the zero degree ply.

In the tests by Naik and Johnson (1991), the fatigue crack patterns show a regular spacing of the cracks. This has also been observed in brittle matrix ceramic composites and other similar composites (Marshall et al., 1985). Cylinder models have been used in conjunction with a shear-lag analysis to calculate the fiber-matrix load transfer in the presence of a fiber or matrix crack. These models have been used to correlate the crack spacing and resulting composite stiffness loss due to cracking in these brittle matrix type composites. The shear-lag analysis has also been used to model the load transfer between plies and predict the crack density in the off-axis plies and the corresponding composite stiffness decrease (Highsmith and Reifsnider, 1982).

In this study, predictions from shear-lag cylinder models are compared to the observed uniform fatigue crack spacing that forms in notched specimens of a continuous fiber $[0/90]_{2S}$ composite. In addition the fatigue crack pattern and fracture surface are examined to gain insight into the initiation and development of fatigue damage in this composite system.

MATERIALS AND METHODS

The material tested in this study was SCS-6/Ti-15-3 composite. The material properties for the matrix and fiber are listed in Table 1. The fiber volume fraction was 0.325. This is the same material system studied extensively by Johnson, et al. (1990) and also tested by Naik and Johnson (1991). The layup tested in this study was $[0/90]_{2S}$, as Naik and Johnson (1991) tested. The center hole specimen was 19mm wide by 1.78mm thick with a 6.35mm diameter hole. The test was run under constant amplitude loading with the maximum stress equal 150 MPa, R equal 0.1 and at 10 Hz frequency. The stress concentration factor for the center hole specimen was calculated by Naik (1991) to be 3.62 taking into account material orthotropy according to Harmon, et al. (1987). The double edge notched specimen was 19mm wide with a 0.4mm by 3 mm deep notch, electro-discharge machined on each side. The elastic stress concentration was determined by Naik (1991) to be 5.97 for $[0/90]_{2S}$ using FEA with orthotropic material properties for the laminates. The fatigue test was run under constant amplitude loading with the maximum stress equal 197 MPa, R equal 0.1 and at 10 Hz frequency. The specimens were polished and surface replicas were made periodically to monitor crack development.

SHEAR-LAG CYLINDER MODELS

The Cox and ACK cylinder models provide the basic shear-lag analysis for predicting the load transfer between the fiber and matrix of a composite (Cox, 1952, Aveston et al., 1971, Aveston and Kelly, 1973). Cox introduced the cylindrical model to help describe the strength of fibrous materials such as paper mat. The ACK model was developed in the early 1970's to help understand the stress-strain curve and type of cracking observed in brittle matrix composite materials like reinforced cements and plasters. The Cox model was derived for a fiber terminating in the matrix, and accounts for the fiber-matrix load transfer along the fiber interface. A similar model is derived in the Appendix for a composite with a matrix crack, which is the problem of interest here.

For a long fiber embedded in the matrix and in equilibrium, part of the load is carried by the matrix and part by the fiber as determined by the law of mixtures. Also, since the strain is the same in the fiber and the matrix there is no shear stress at the interface. If either the matrix or the fiber fails, a mismatch in strain between the fiber and matrix is created which causes a corresponding shear stress acting along the fiber-matrix interface. This interface shear stress is a maximum at the crack and decreases along the fiber until there is no strain mismatch. If the matrix had failed, then the stress in the matrix increases from zero at the crack to the steady state composite value at some distance along the fiber. This load transfer between the fiber and matrix is the problem solved with the cylinder models using the shear-lag analysis.

The basic shear-lag assumption is that the load transfer between fiber and matrix at any point along a bonded interface is directly proportional to the relative displacement between the fiber and the matrix. Considering a crack in the matrix, this becomes

$$\frac{dP_m}{dx} = H(u - v) \tag{1}$$

where P_m = force in matrix
x = distance from crack along the fiber
H = constant
u = displacement in matrix
v = displacement in fiber

Cox Model for a Matrix Crack

The model developed in the Appendix follows the Cox derivation with complete fiber-matrix bonding, however with a crack in the matrix. In the basic cylinder model shown in Figure A-1, r_f is the fiber radius and R is the radius of an equivalent matrix which provides the composite matrix volume ratio, V_m. The resulting axial matrix stress, σ_m, and interface shear stress, τ, along the fiber length are as follows:

$$\sigma_m = E_m \varepsilon \left[1 - \frac{\cosh[\beta(L-x)]}{\cosh(\beta L)} \right] \tag{2}$$

$$\tau = - \frac{E_m A_m \beta \varepsilon}{2\pi r_f} \left[\frac{\sinh[\beta(L-x)]}{\cosh(\beta L)} \right] \tag{3}$$

where $\beta = \left[\frac{2\pi G_m}{E_m A_m \ln(R/r_f)} \right]^{1/2}$

and E_m = matrix modulus
A_m = matrix area
r_f = fiber radius
L = bond length
R = equivalent cylinder radius
ε = composite strain
E_f = fiber modulus
V_f = fiber volume fraction
V_m = matrix volume fraction

The above solution to the differential is a periodic exponential function which is illustrated in Figure 3. This shows the build up in axial matrix stress for matrix cracks located at x = 0 and x = 2L. The corresponding interface shear stress is a maximum at the crack and decreases exponentially.

Aveston, Cooper and Kelly (ACK) Model (1971, 1973)

The ACK model also uses the basic shear-lag assumption with a cylinder model (equation (1)). This model considers three conditions as follows:

Condition i: Completely Debonded Interface. For this case complete debonding along the entire length of the fiber is assumed and, in addition, fiber-matrix load transfer is assumed to be achieved by a constant shear stress at the interface due to friction. This gives

$$\frac{dP_m}{dx} = 2\pi r_f \tau \tag{5}$$

where P_m = matrix force

Condition ii: Complete Fiber–Matrix Bonding. The completely bonded case utilizes the shear-lag model and assumes that when the matrix fails, the load it previously carried is now transferred entirely to the fiber within the cylinder, whereas in the Cox model it was assumed that the load was transferred to the remaining composite. For complete bonding, the ACK model gives

$$\sigma_m = \frac{V_f}{V_m}(\Delta\sigma_o)\left[1 - e^{-\phi^{1/2}x}\right] \tag{6}$$

$$\tau = \frac{r_f}{2}(\Delta\sigma_o)\phi^{1/2}e^{-\phi^{1/2}x} \tag{7}$$

where

$$\phi^{1/2} = \left[\frac{2G_m E_c}{E_f E_m V_m}\right]\frac{1}{r_f\left[\ln(R/r_f)\right]^{1/2}} \tag{8}$$

and $\Delta\sigma_o = \dfrac{\sigma_c}{V_f} - \varepsilon E_f$

σ_c = composite stress

ε = composite strain

Condition iii: Partially Bonded Interface. In the bonded case, the interface shear stress is a maximum at the matrix crack, where $x = 0$. If this shear stress exceeds the interface shear strength, τ_u, debonding will occur and the load transfer between the fiber and matrix over the debond region is assumed to be due to a constant shear stress, τ'. Debonding occurs along the fiber until the remaining load to be transferred is such that $\tau_{max} \leq \tau_u$. The total length, L, over which the load is transferred, is the sum of the debonded region plus the elastic bonded region. It depends on the interface shear strength, τ_u, and the debond shear stress, τ'. This is illustrated in Figure 4. This results in the following for the matrix and interface shear stresses:

$$\sigma_m = \frac{2\pi r_f x'\tau'}{V_m} + \frac{1}{V_m}\left[V_f\Delta\sigma_o - 2\pi r_f x'\tau'\right]\left[1 - e^{-\phi^{1/2}(x-x')}\right] \tag{9}$$

$$\tau = \tau' \qquad \text{for } 0 < x < x'$$

$$\tau = \frac{r_f}{2}\left[\Delta\sigma_o - \frac{2\pi r_f x'\tau'}{V_f}\right]\phi^{1/2} e^{-\phi^{1/2}(x-x')} \quad \text{for } x' < x < L \tag{10}$$

RESULTS AND DISCUSSION

Cylinder Models

The Cox and ACK models are very similar, differing only in the form of the solution. In both models, the elastic load carried in the matrix increases exponentially as we move away from the matrix crack. The fiber-matrix load transfer distance, L, is the distance required for the fiber to transfer the load to the matrix and bring the matrix stress up to the intact composite value, σ_m^{∞}. The expected minimum crack spacing is 2L (Figure 4).

The stress transfer to the matrix approaches σ_{max}^{∞} asymptotically which means that under a static load a further increase in load would be necessary for an additional crack to form. However, under constant amplitude fatigue loading, multiple matrix cracks will develop without an increase in load because the fatigue crack formation is occurring as a cumulative process at the same load. It is interesting to note that for the completely bonded case the models show that the crack spacing is dependent on the fiber and matrix moduli as given by the parameter, ϕ, and independent of the applied load level. The length, L, over which elastic load transfer occurs is given by the exponential term in equation (6), which for 100 percent load transfer, L is infinite. However, for practical purposes the load can be considered to be transferred when

$$\left[1 - e^{-\phi^{1/2}x}\right] = M \tag{11}$$

where M is a number slightly less than 1.

When ϕ is large, the load transfer occurs over a shorter distance creating a higher interface shear stress, which in turn, increases the tendency for debonding to occur. Also, the maximum interface shear stress, τ_{max}, which occurs at x equal 0 is directly proportional to the applied load. If τ_{max} exceeds the interface bond strength, τ_u, in Figure 4, then debonding occurs. If the load is sufficiently large, complete debonding can occur.

Fatigue Crack Pattern

Figure 5 shows the fatigue crack pattern for the center hole specimen after 200,000 cycles at σ_{max} equal 150 MPa. The crack pattern about 1mm from the center hole shows a uniform spacing of 0.5 to 0.6mm. This is also close to the observed crack spacing for Naik and Johnson's (1991) specimen shown in Figure 1.

Fatigue cracks initiated approximately 1mm from the maximum stress point in the center hole specimen (points A and C in Figure 5). X-ray and SEM studies of the fracture surface showed that these locations are where the first cut fiber intersects the hole. This creates a local stress concentration in the matrix causing a crack to develop at this point. As the cracks grow out from the hole, additional cracks begin to form in between these predominate cracks at a uniform distance apart.

Naik and Johnson (1991) also observed debonding of the fiber-matrix interface near the hole (Figure 2), which can increase the distance over which the full fiber-matrix load transfer occurs, and thereby increase the crack spacing. The stress is higher near the notch and more debonding will occur, resulting in a larger crack spacing near the notch. This can be observed in both Figures 5 and 6 for the center hole and edge notch specimens. The maximum debond length for the fiber shown in Figure 2 is 0.17mm. The crack spacing observed in the edge notch specimen shows a uniform spacing of about 0.8mm at a short distance in from the notch (Figure 6). The cracks initiating at the notch and running parallel to the zero degree fiber observed in the edge notch specimen are due to the high shear stress causing matrix crack growth parallel to the fibers (Harmon, et al., 1987).

Comparison of Cylinder Models with Experimental Observations

Near the notch, the stress appears to be large enough for debonding to occur as observed in Figure 2. In the center hole specimens tested in this study and by Naik and Johnson (1991), the characteristic crack spacing at locations removed from the notch is about 0.5mm. If we assume that at this spacing, the fiber matrix interface is fully bonded, then for the ACK model the maximum stress is 0.975 of σ_m^∞ (M = 0.975 in equation (11)) and for the Cox model M = 0.94. As previously mentioned the crack spacing is independent of the applied stress level for the fully bonded case. However, when debonding occurs the crack spacing can correspondingly increase. Therefore it is likely that the observed 0.5mm crack spacing is for the fully bonded condition and is due to the uniform applied stress level.

The expected debond length at the edge of the hole (Figures 2 and 5) can be determined as follows. The crack spacing of 0.5mm is assumed to be for complete bonding and subjected to the specimen applied stress level. The maximum shear stress, τ_{max}, at the interface as determined from equation (7) is 76 MPa at x = 0.

The shear strength, τ_u, is assumed to be equal to this τ_{max} value. The constant frictional shear strength in the debond region, τ', is also assumed to be equal to τ. Applying the stress concentration factor of 3.62 for the center hole and solving equation (9) for x' gives the expected debond length at the edge of the hole. These results are

Calculated debond length:	0.18mm
Maximum value observed from Figure 2:	0.17mm

This debond length gives a predicted crack spacing of 0.86mm which compares with that observed in regions of uniform spacing near the hole and notch in Figures 5 and 6.

Fractograph Observations

In the $[0/90]_{2S}$ laminate it is possible that fatigue cracks could initiate in the 90-degree layer and progress through the zero-degree ply to the surface. Small discontinuous cracks were observed on the surface which later joined to form a continuous crack. This can be seen in Figures 5 and 6. Also, SEM study of the surface showed one location where discontinuous cracks parallel to the 90-degree fibers were one fiber spacing apart.

The center hole specimen, after 200,000 cycles, was loaded to fracture and the fracture surface examined with the SEM. The failure occurred at crack A shown in Figure 5. The first failed fiber at this location is shown in Figure 7. The radial lines extending out from the fiber indicate that the crack initiated around the fiber and grew radially. In this fractograph, there is no evidence of crack initiation in the 90-degree ply. This was the general appearance at most of the 0-degree fibers, especially near the notch. Figure 8 shows a point about 1mm further along the same 90-degree fiber. The feather areas emanating from the 90-degree fiber appear to be areas of crack initiation along the fiber, which do not appear to progress through to zero degree fibers in the next ply. The observation that the cracks initiated around the fibers substantiates that the stress in the zero-degree fiber is a controlling parameter in the matrix crack initiation and growth processes. Kantzos et al. (1989), in tests run under direct SEM observation, also observed crack initiation around the fibers in $[0]_8$ layups of the same material. They also concluded that in many cases the crack initiated in the carbon layer surrounding the fiber.

Even where cracks initiated in the 90-degree ply, they did not progress through the 0-degree ply, and therefore the crack spacing would not be expected to change. This is because the build-up of matrix stress as predicted by the models is necessary to propagate the crack through the zero-degree ply.

The fractograph in Figure 9 shows the two adjoining 90-degree fibers in the center of this $[0/90]_{2S}$ layup. The top half of the fractograph shows the fatigue crack region and the lower half shows the ductile rupture where it was pulled to fracture. The fatigue crack appears to have progressed along and out from these two center 90-degree fibers. However these cracks do not appear to have propagated through the adjoining 0-degree plies.

SUMMARY

1. In regions removed from the notch tip, the Cox and ACK models provide a good correlation of the crack spacing assuming no debonding at the fiber-matrix interface.

2. The ACK model for a partially debonded condition correlates well with the observed debond length.

3. Higher stresses near the notch cause fiber-matrix debonding which increases the crack spacing.

4. SEM fractographs indicate that the matrix fatigue cracks initiated predominantly around the zero-degree fibers.

5. Failure of the fiber-matrix bond in the 90-degree ply does not appear to influence fatigue crack development.

ACKNOWLEDGEMENTS

The authors would like to acknowledge M.H. Swain of Lockheed Engineering and Sciences Co., Hampton, VA and R.A. Naik of Analytical Services and Materials, Inc., Hampton, VA for their assistance with the SEM studies and stress concentration analysis, respectively.

REFERENCES

1. Aveston, J., Cooper, G.A., and Kelly, A., 1971, "The Properties of Fibre Composites," Conference Proceedings, National Physical Laboratory IPC Science and Technology Press Ltd., Paper I, p 15.

2. Aveston, J. and Kelly, A., 1973, "Theory of Multiple Fracture of Fibrous Composites," J. Mat. Sci., Vol. 8 pp 352-362.

3. Cox, H.L., 1952, "The Elasticity and Strength of Paper and Other Fibrous Materials," British J. Appl. Physics, Vol. 3, p 72.

4. Harmon, D.M., Saff, C.R. and Sun, C.T., 1987, "Durability of Continuous Fiber Reinforced Metal Matrix Composites," AFWAL-TR-87-3060, Wright-Patterson Air Force Base, Ohio, October.

5. Highsmith, A.L. and Reifsnider, K.L., 1982, "Stiffness-Reduction Mechanisms in Composite Laminates," Damage in Composite Materials, ASTM STP 775, Am. Soc. Test. Mat.

6. Johnson, W.S., Lubowinski, S.J. and Highsmith, A.1., 1990, "Mechanical Characterization of Unnotched SCS-6/Ti-15-3 Metal Matrix Composites at Room Temperature," Thermal and Mechanical Behavior of Ceramic and Metal Matrix Composites, ASTM STP 1080, Am. Soc. Test. Mat.

7. Kantzos, P. Telesman, J. and Ghosn, L., 1989, "Fatigue Crack Growth in a Unidirectional SCS-6/Ti-15-3 Composite," NASA TM 103095, NASA Lewis Research Center Group.

8. Marshall, D.B., Cox, B.N. and Evans, A.G., 1985, "The Mechanics of Matrix Cracking in Brittle-Matrix Fiber Composites," Acta Met., Vol. 3, No. 11, pp 2013-2021.

9. Naik, R.A. and Johnson W.S., 1991, "Observations of Fatigue Crack Initiation and Damage Growth in Notched Titanium Matrix Composites," Third Symposium on Composite Materials: Fatigue and Fracture, ASTM STP 1110, In press, Am. Soc. Test. Mat.

Table 1. SCS-6/Ti-15-3 Properties

Fiber Modulus:	400 GPa
Fiber Poisson's ratio:	0.25
Matrix Modulus:	92.5 GPa
Matrix Poisson's ratio:	0.35
Matrix yield:	690 GPa
Matrix ultimate:	934 GPa
Fiber diameter:	0.142 mm
Fiber volume fraction:	0.325

APPENDIX: COX MODEL FOR A MATRIX CRACK

Cox assumed the basic shear-lag condition in which the load transferred between the fiber and matrix is proportional to the difference between the displacement of the matrix and the fiber. For the case of a matrix crack, the force in the matrix, P_m, is

$$\frac{dP_m}{dx} = H(u-v) \tag{A-1}$$

where u = the displacement in the matrix,
v = the displacement in the fiber
H = constant.

Differentiating equation A-1 gives

$$\frac{d^2P_m}{dx^2} = H\left[\frac{du}{dx} - \frac{dv}{dx}\right] \tag{A-2}$$

The strain in the fiber is assumed to be equal to the average strain in the composite, which implies that the load previously carried by the matrix is carried by the remaining composite and no additional load is transferred to the fiber. Therefore,

$$\frac{dv}{dx} = \varepsilon_f = \varepsilon \tag{A-3}$$

and

$$\frac{du}{dx} = \varepsilon_m = \frac{P_m}{E_m A_m} \tag{A-4}$$

assuming a homogeneous matrix stress state in the radial direction. A_m is the matrix area. Substituting equations (A-3) and (A-4) into (A-2) gives,

$$\frac{d^2P_m}{dx^2} = H\left[\frac{P_m}{A_m E_m} - \varepsilon\right] \tag{A-5}$$

which has a solution of the form

$$P_m = E_m A_m + R\cosh(\beta x) + S\sinh(\beta x) \tag{A-6}$$

where $\beta = \left[H/E_m A_m\right]^{1/2}$

The boundary conditions are

$$P_m = 0 \text{ at } x = 0,2L \tag{A-7}$$

which gives

$$\sigma_m = E_m \varepsilon \left[1 - \frac{\cosh\left[\beta(L-x)\right]}{\cosh(\beta L)} \right] \tag{A-8}$$

If τ is the interface shear stress at some position, x, along the fiber, then from equilibrium in the x direction

$$\frac{dP_m}{dx} = -2\pi r_f \tau \tag{A-9}$$

where $r_f$is the fiber radius.

Letting dw/dx be the shear strain in the matrix at some position x, then

$$\frac{dw}{dr} = \frac{\tau}{G_m} \tag{A-10}$$

which is integrated from r_f to R

$$\Delta w = \frac{\tau r_f}{G_m} \ln(R/r_f) \tag{A-11}$$

where G_m is the matrix shear modulus. However, $\Delta w = (u-v)$ and along with combining equations (A-9) and (A-1) gives

$$H = \frac{2\pi G_m}{\ln(R/r_f)} \tag{A-12}$$

and

$$\beta = \left[\frac{2\pi G_m}{E_m A_m \ln(R/r_f)} \right]^{1/2} \tag{A-13}$$

Differentiating equation (A-6) and substituting into (A-9) give the shear stress at the fiber-matrix interface

$$\tau = -\frac{E_m A_m \beta \varepsilon}{2\pi r_f}\left[\frac{\sinh[\beta(L-x)]}{\cosh(\beta L)}\right] \qquad \text{(A-14)}$$

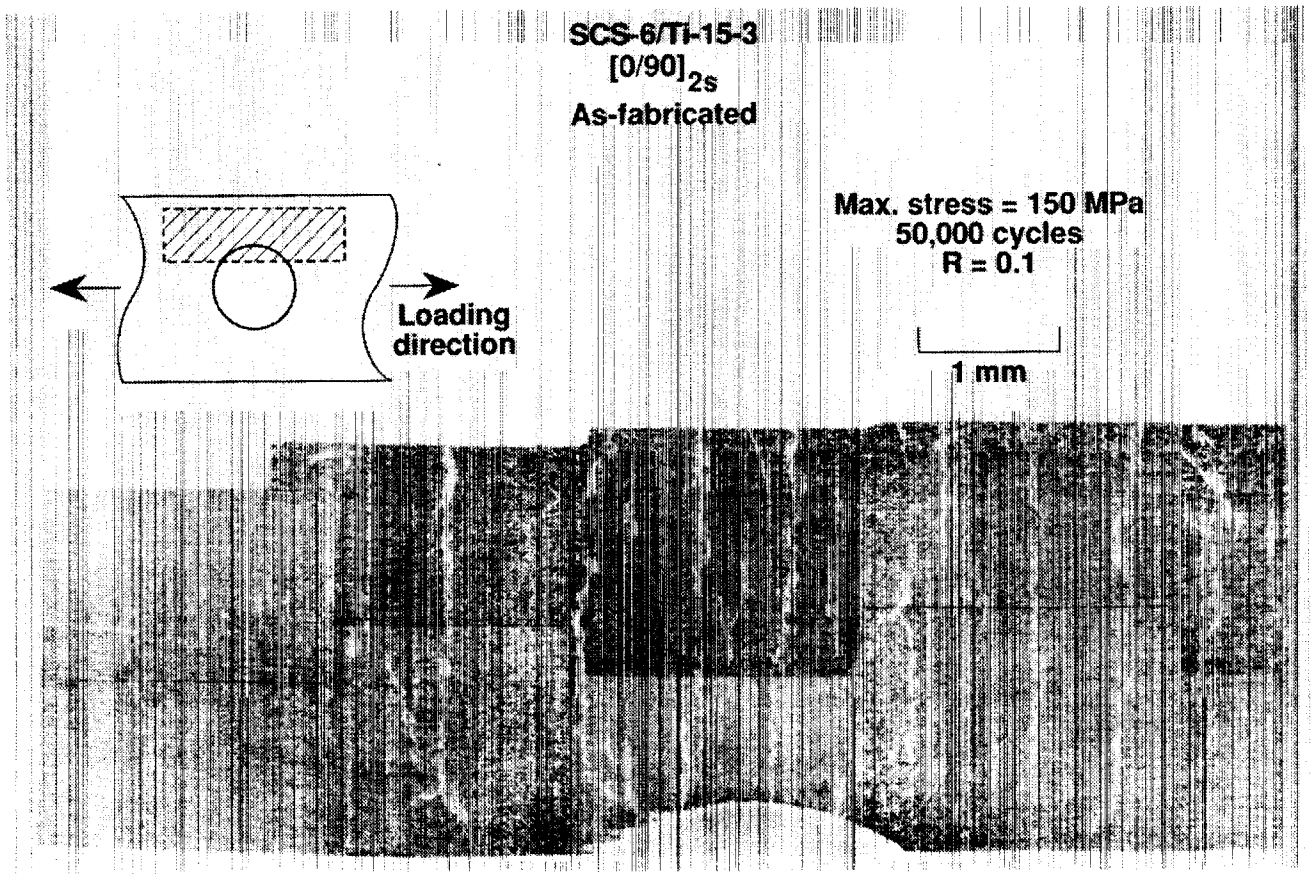

Figure 1. Matrix fatigue cracks near center hole stress raiser in specimen tested by Naik and Johnson (1991).

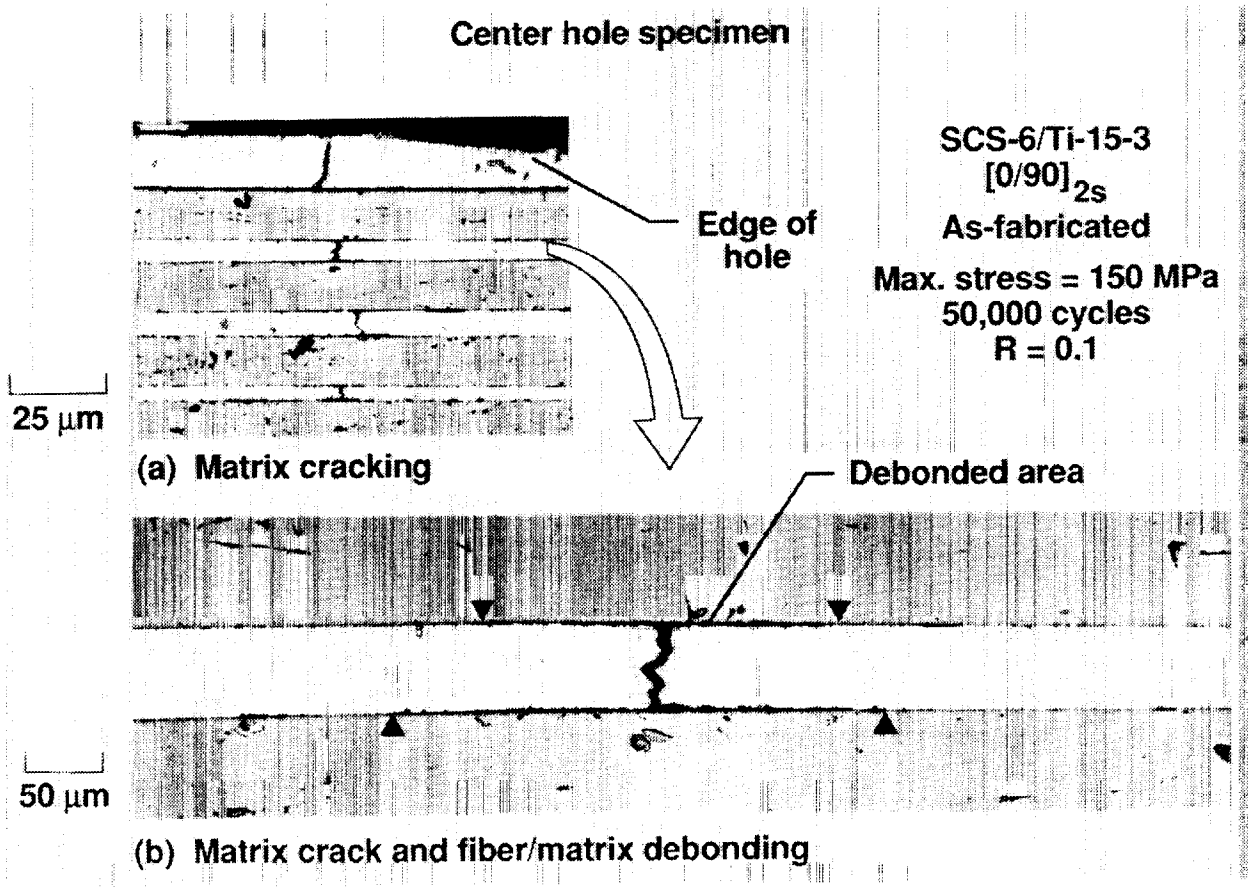

Figure 2. Fiber-matrix interface separation at matrix fatigue crack observed by Naik and Johnson (1991).

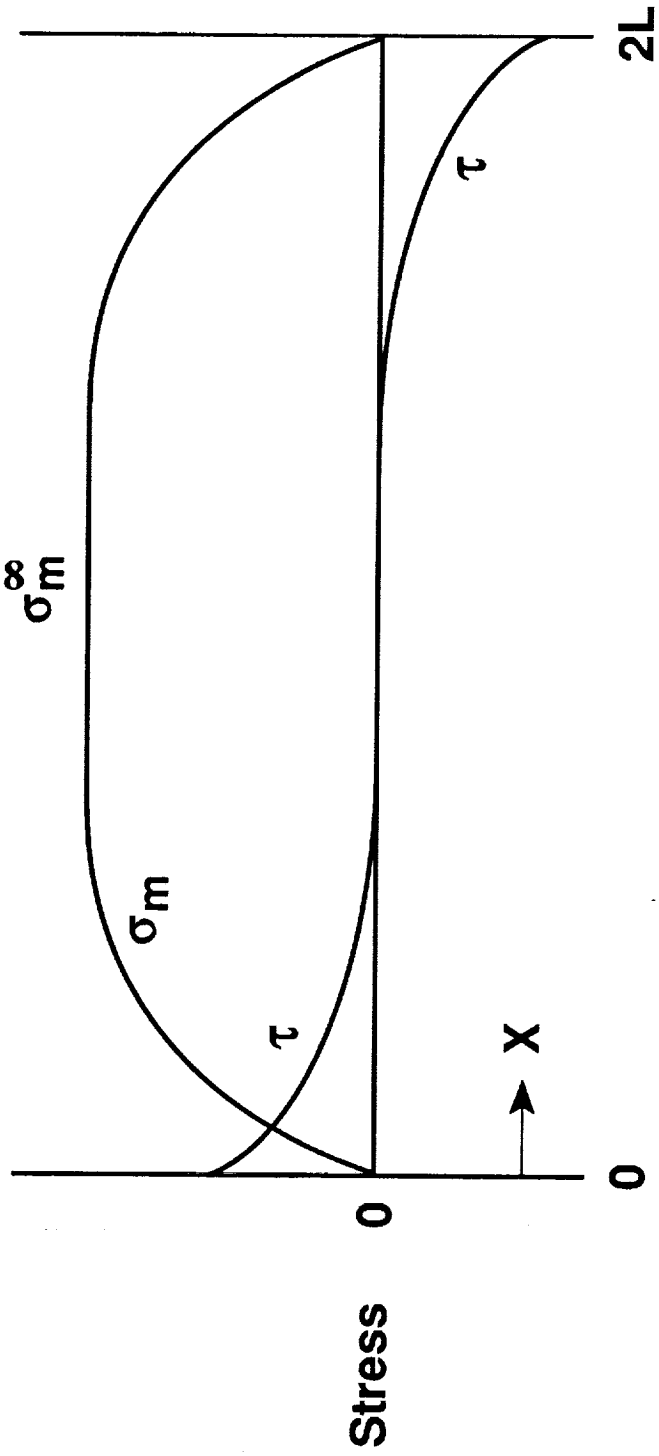

Figure 3. Matrix stress and interface stress as a function of the distance between cracks, 2L.

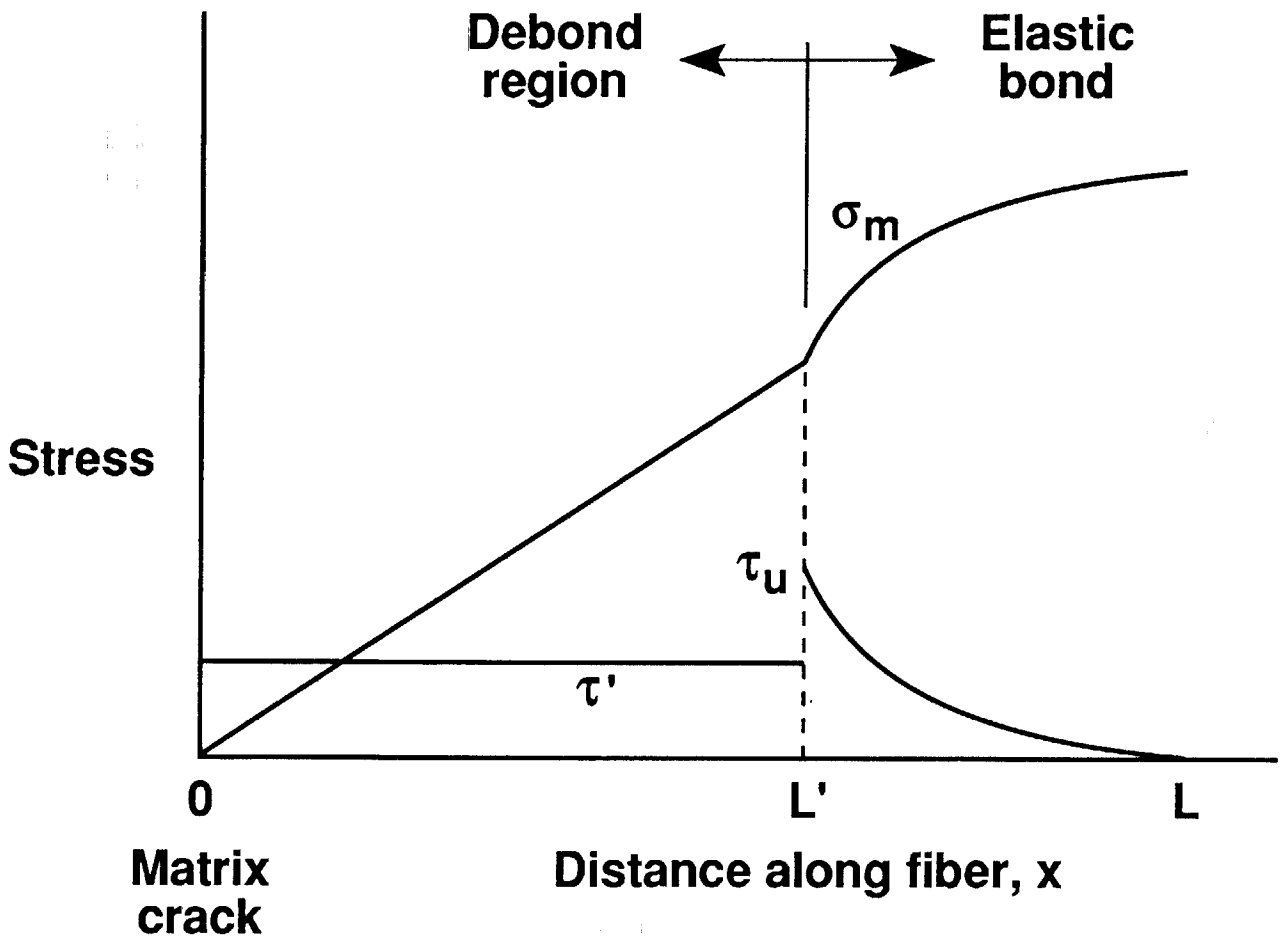

Figure 4. Stress transfer between matrix and fiber with partial debonding.

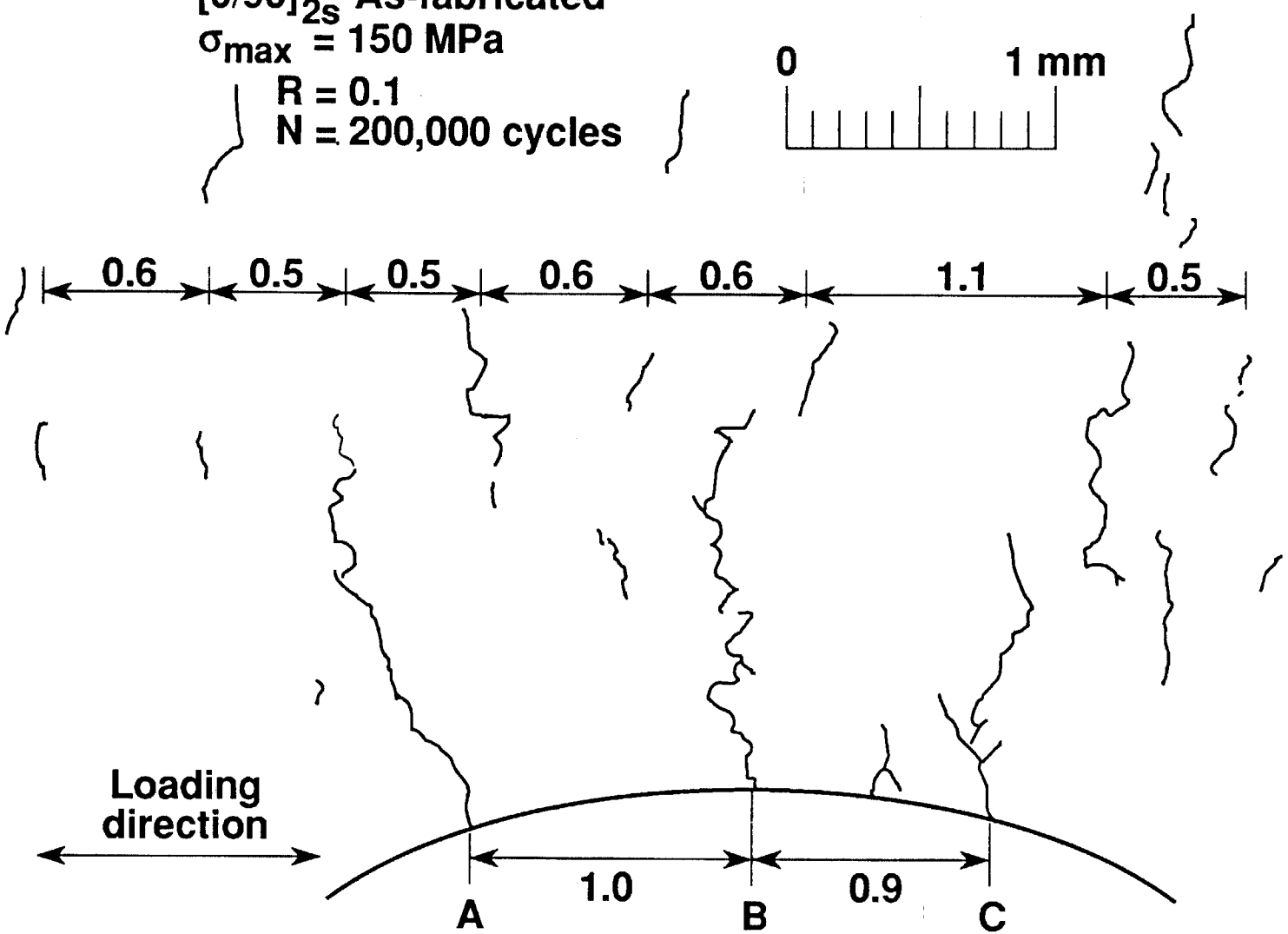

Figure 5. Fatigue crack pattern in center-hole specimen.

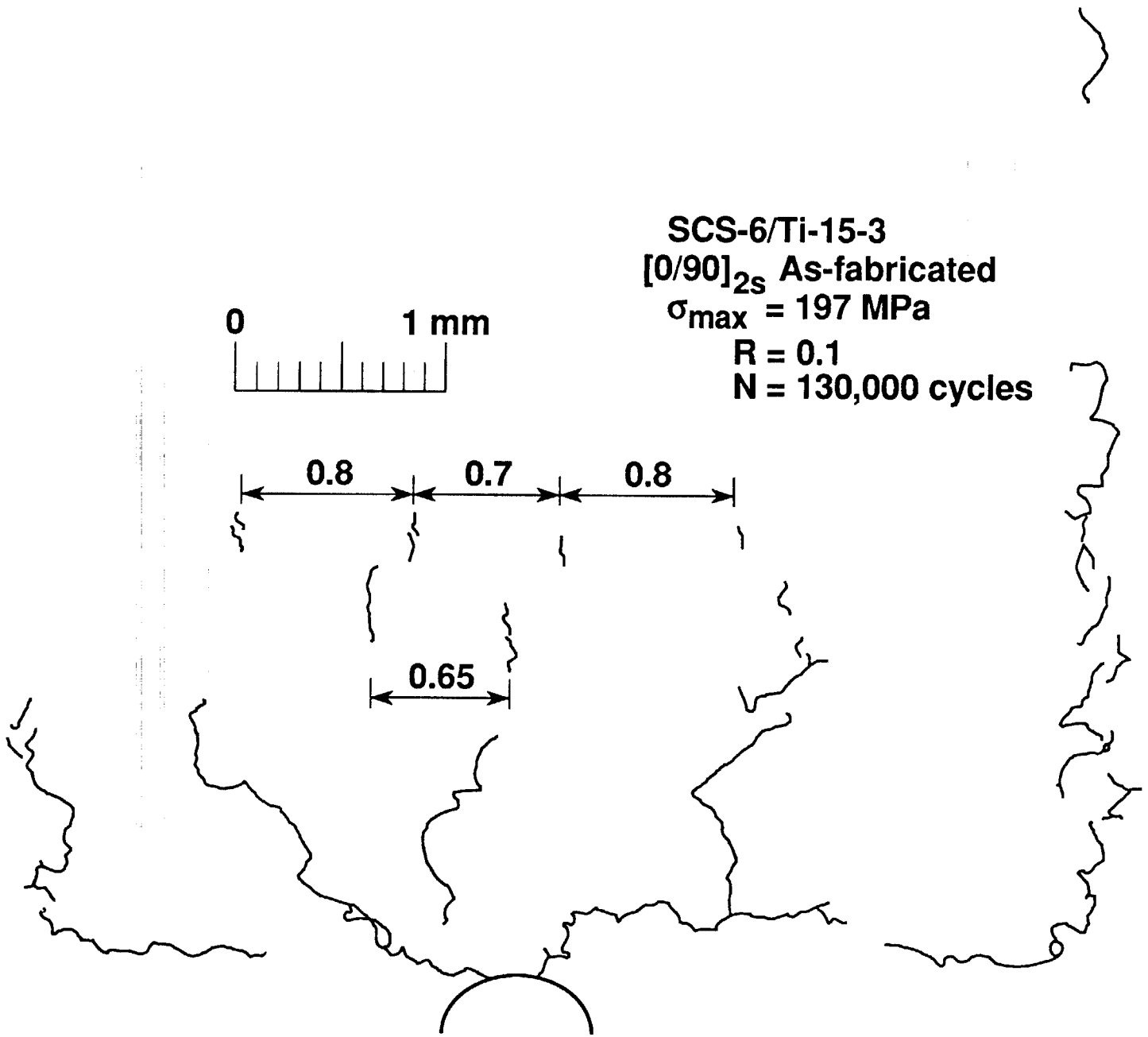

Figure 6. Fatigue crack pattern in double edge-notch specimen.

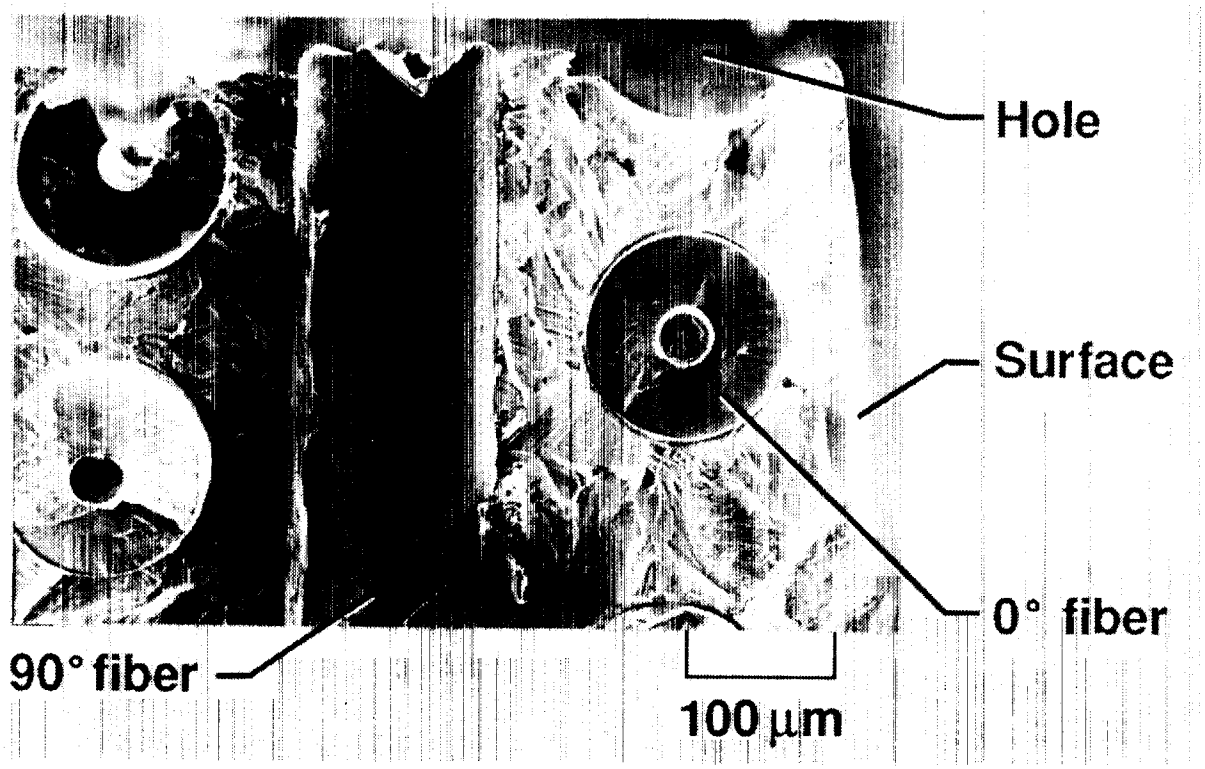

Figure 7. Fractograph showing crack initiation around the first zero-degree fiber at location A in figure 5. Loading direction is perpendicular to the photograph.

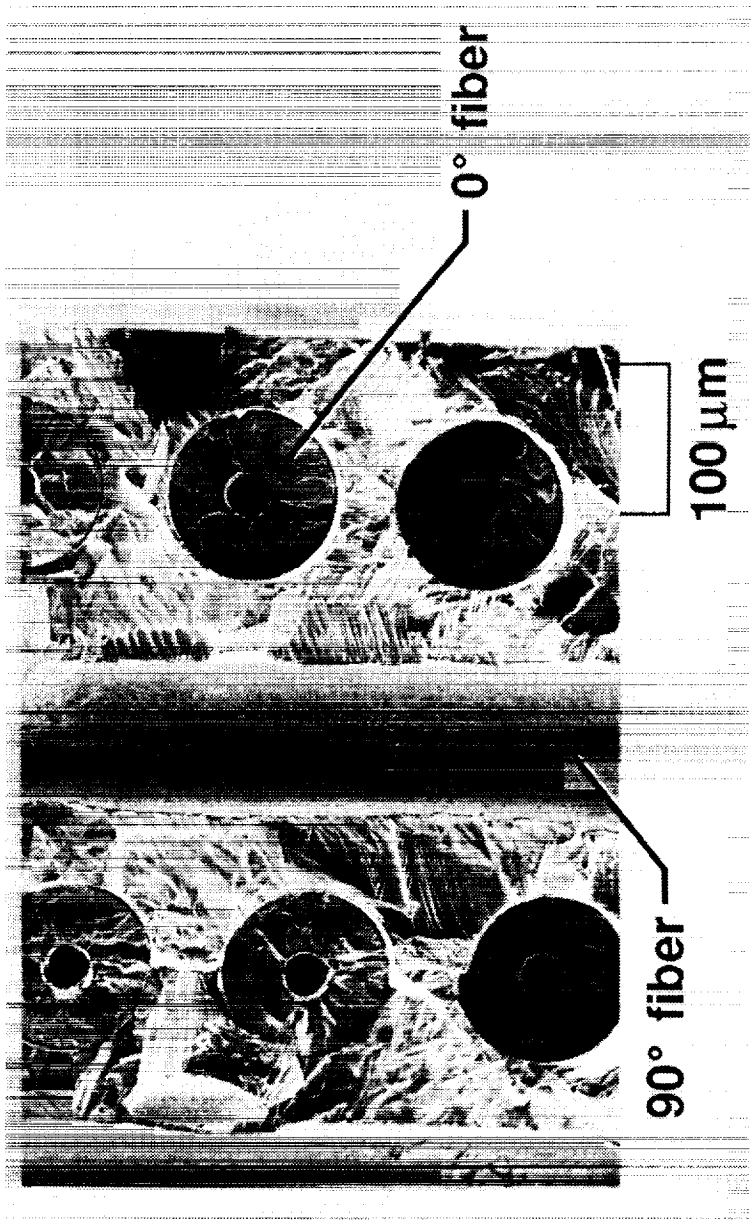

Figure 8. Fractograph of same fatigue crack as in Figure 7, farther along the 90-degree fiber.

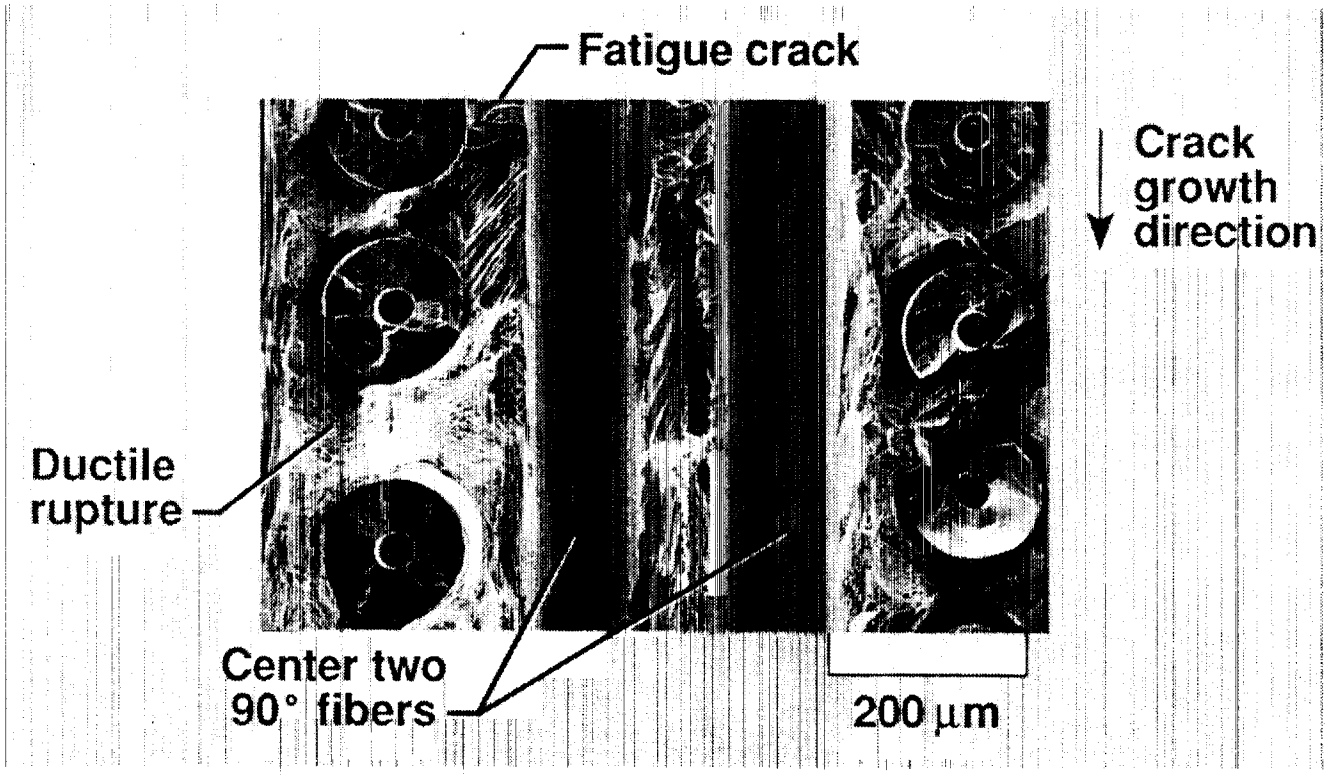

Figure 9. Fractograph showing fatigue crack growth along two adjoining 90-degree fibers in the center of the laminate. Ductile rupture can also be seen in the lower portion of the photograph.

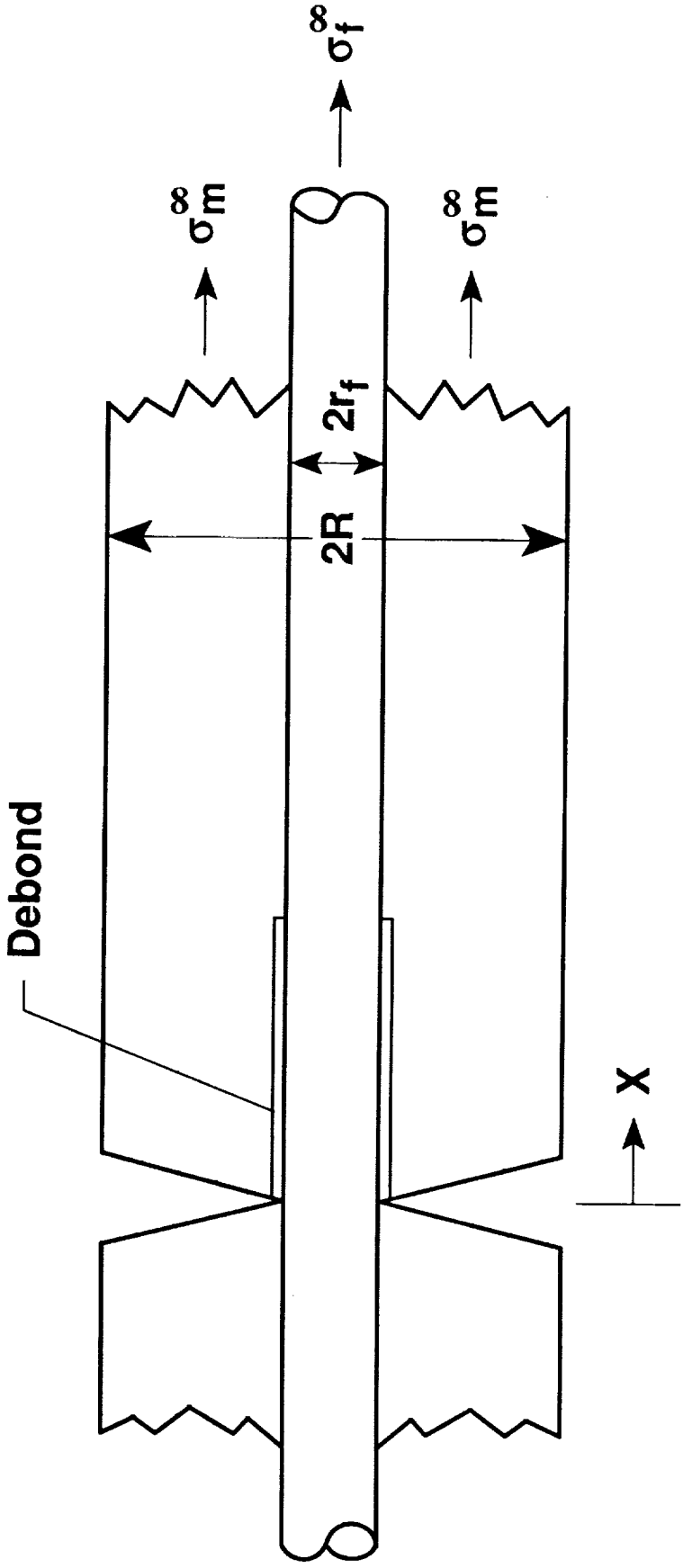

Figure A-1. Cylindrical model for a matrix crack.

NASA
National Aeronautics and Space Administration

Report Documentation Page

1. Report No.	2. Government Accession No.	3. Recipient's Catalog No.
NASA TM-102751		

4. Title and Subtitle

Matrix Fatigue Crack Development in a Notched Continuous Fiber SCS-6/Ti-15-3 Composite

5. Report Date

November 1990

6. Performing Organization Code

7. Author(s)

B. M. Hillberry[1] and W. S. Johnson[2]

8. Performing Organization Report No.

10. Work Unit No.

506-43-71-01

9. Performing Organization Name and Address

NASA Langley Research Center
Hampton, VA 23665-5225

11. Contract or Grant No.

13. Type of Report and Period Covered

Technical Memorandum

12. Sponsoring Agency Name and Address

National Aeronautics and Space Administration
Washington, DC 20546-0001

14. Sponsoring Agency Code

15. Supplementary Notes

[1]National Research Council Senior Research Associate, NASA Langley Research Center.
[2]Senior Research Engineer, NASA Langley Research Center.
This paper will be presented at the ASME Winter Annual Meeting, Dallas, TX, November 1990.

16. Abstract

In this study the extensive matrix fatigue cracking that has been observed in notched SCS-6/Ti-15-3 composites is investigated. Away from the notch a uniform spacing of the fatigue cracks develops. Closer to the notch, fiber-matrix debonding which occurs increases the crack spacing. Crack spacing and debond length determined from shear-lag cylinder models compare favorably with experi- mental observations. SEM fractography showed that the principal fatigue crack initiation occurred around the zero degree fibers. Interface failure in the 90-degree plies does not lead to the development of the primary fatigue cracking.

Scanning electron microscope

17. Key Words (Suggested by Author(s))	18. Distribution Statement
Crack spacing Shear transfer Micromechanics Cylinder model Titanium matrix composite	Unclassified - Unlimited Subject Category - 24

19. Security Classif. (of this report)	20. Security Classif. (of this page)	21. No. of pages	22. Price
Unclassified	Unclassified	24	A03